

Investigation using single point incremental forming (SPIF) to fabricate patient-specific, titanium orbital floor implants

Elizabeth M. Mamros^{1*}, Lauren E. Blaha², and Christian A. Kauffman²

¹Department of Mechanical Engineering, Bucknell University, Lewisburg, PA, 17837, USA

²Plastic and Reconstructive Surgery, Geisinger Medical Center, Danville, PA, 17822, USA

Abstract. The floor of the human orbit is composed of thin bone that is prone to traumatic fracture. This leads to a loss of support for the eye, which can cause vision changes. Therefore, fractures may need surgical reconstruction using a thin, sheet-like implant. Titanium implants are available off-the-shelf in standard sizes, but fitting to each patient's unique anatomy requires surgeons to cut, file, and bend these plates. This can be time-consuming and imprecise. To both save time and ensure a perfect fit for the patient, a custom plate can be created prior to surgery. This investigation focuses on single-point incremental forming as a novel technique to fabricate patient-specific orbital floor implants. This method for sheet metal forming of biocompatible titanium (commercially pure grade 2) is faster, more flexible, and creates less waste than conventional methods. Implant geometry can be manipulated by modifying the toolpath and process parameters. This allows customization to match the patient's precise anatomy, resetting the eye to an appropriate position. The microstructure of the formed part can also be controlled, increasing strength in fixation areas. Incremental forming has the potential to revolutionize the implant manufacturing industry through the generation of functionally-graded components.

Keywords: Single point incremental forming; Titanium; Customization; Medical application.

1 Introduction

To meet the customization requirements of the medical industry, incremental forming is one method currently under investigation to fabricate patient-specific implants. Single point incremental forming (SPIF) is a sheet metal forming process, which typically involves a hemispherical tool locally deforming a workpiece in a layer-by-layer manner, following a user-defined toolpath. SPIF is a flexible manufacturing process, which does not require custom tooling, e.g., dies, and can allow for geometrical changes by manipulating the machine code or toolpath. This flexibility enables rapid production of implants that are anatomically-matched to each patient in less time than what is required for additive manufacturing. Heron et al. [1] reported that 3D-printing accounted for the most time-intensive step in the pre-operative workflow. Incremental forming offers an opportunity to both improve the pre-operative workflow and enable surgeons to have access to custom implants faster.

The majority of SPIF research has focused on cranial implants using biocompatible materials, such as stainless steel [2], titanium [3], ultrahigh molecular weight polyethylene (UHMWPE) [4], and polyetheretherketone (PEEK) [5]. In addition to biocompatibility, material properties that are desirable for this medical application include elastic modulus similar to that of bone, low density, non-magnetic, low

thermal conductivity, and high corrosion resistance. There have been a few investigations into other types of implants, including frontal bone and mandible [6], denture bases [7], clavicle [8], ankle support [9], knee [10], and hip [11]. All of these studies provide support for shifting the custom implant industry from machining and additively manufacturing implants to using incremental forming as their primary manufacturing process. However, there are remaining challenges with regards to processing biocompatible materials, obtaining acceptable geometrical accuracy, and acquiring the appropriate approvals required for human trials.

Recently, Rosa-Sainz et al. [12] studied the influence of SPIF process parameters on the formability of PEEK at room temperature for cranial and cheek bone prosthetics. Bagudanch et al. [4] evaluated the cost and environmental impact associated with a polymer implant fabricated by SPIF and found the process to be a cheaper alternative to traditional methods with a low lead time. Piccininni et al. [13] reported success with using both super plastic forming and SPIF approaches to manufacturing titanium implants. Thauker and Chauhan [14] investigated using perforated titanium sheets for SPIF to promote osteointegration and reduce the number of post-processing steps required for implants.

This paper focuses on using SPIF for a much smaller implant than those studied previously – the orbital floor. The bony floor that supports the eyeball

* Corresponding author: emm047@bucknell.edu

(globe) is prone to fracture as a result of blunt force injury. Large fractures can lead to long-term visual issues and must be repaired surgically with the placement of an orbital floor implant. This implant is intended to be permanent, providing lifelong support for the globe. An example of commercial orbital floor implants is shown in Fig. 1.



Fig. 1. Commercial orbital floor implants [15].

In the present study, a procedure is described for designing an orbital floor implant starting with a patient’s computed tomography (CT) scan. This patient-specific implant is then formed with commercially-pure titanium (CP-Ti) grade 2 sheets subjected to SPIF at room temperature. The geometrical accuracy of the implant is assessed and suggestions are made for future improvements and investigations. This work describes the first known production of a patient-specific orbital floor implant using SPIF, expanding the portfolio of possibilities for small-scale titanium SPIF.

2 Methods and procedures

CP-Ti grade 2 sheets with a thickness of 0.5 mm were used for the experiments described in the following sections. The elemental composition provided by the manufacturer is shown in Table 1.

Table 1. CP-Ti grade 2 elemental composition [percent].

Fe	C	N	H	O	Ti
0.050	0.008	0.004	0.003	0.090	99.845

The specimen geometries for the material characterization and SPIF experiments are shown in Fig. 2. Specimens were extracted using abrasive waterjet cutting according to the specified dimensions. All cut edges were lightly deburred prior to experiments.

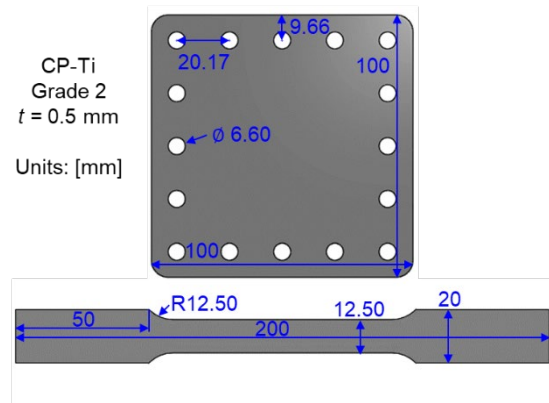


Fig. 2. Specimen geometries for incremental forming (top) and uniaxial tension (bottom) experiments.

A stereo-digital image correlation (DIC) system was used for all experiments. The system included two 5.0 megapixel cameras with 8 mm (SPIF) and 17 mm (uniaxial tension) focal length lenses (Schneider-Xenoplan), and post processing was completed in VIC-3D (Correlated Solutions Inc.). Subset and step sizes of 29 and 7, respectively, were used for all analyses. Images were acquired at a rate of 1 Hz, focusing on the gauge area of the tensile specimens and on the non-toolside of the specimens for SPIF. Both types of specimens were prepared with a black speckle pattern on top of a white spray-painted background for detection in the DIC software. A rubber stamper and ink pad were used to create the black speckle pattern.

2.1 Material characterization

Uniaxial tension (UT) tests were conducted, according to the ASTM E8 standard [16], using a universal testing machine (Instron) with a 300 kN load cell as shown in Fig. 3. The displacement rate was set to 0.1 mm/s, which corresponds to a strain rate of approximately 0.001 s⁻¹. Specimens were oriented at 0°, 45°, and 90° with respect to the rolling direction. Three repetitions were completed for each orientation to ensure repeatability.

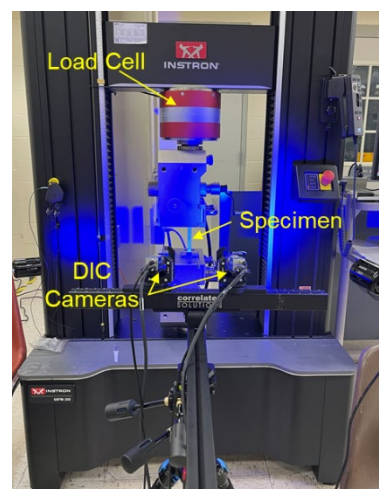


Fig. 3. Uniaxial tension test experimental setup.

2.2 Single point incremental forming (SPIF)

The SPIF experiments were conducted using a TorqueCut 22 (Bridgeport) computer numerical control (CNC) machining center with a custom frame as shown in Fig. 4. The hole pattern shown in Fig. 2 for the incremental forming specimens aligns with bolts in the fixture to securely clamp the sheet, and creates a 70 mm x 70 mm forming (unclamped) area. A 2 mm diameter hemispherical tool made of hardened A2 tool steel was used with multi-purpose synthetic grease (Super Lube NLGI) spread in a thin layer across the sheet metal for lubrication, and the sheet was oriented with the rolling direction along the x-axis shown in Fig. 4. The toolpath was programmed in Mastercam 2024 using a surface finishing contour operation, feed rate of 635 mm/min, spindle speed of 25 rpm, conventional milling, and a maximum stepdown of 0.1 mm. The forming time was approximately 20 minutes. Note that this speed could be improved for eventual industrial applications by optimizing the toolpath parameters.

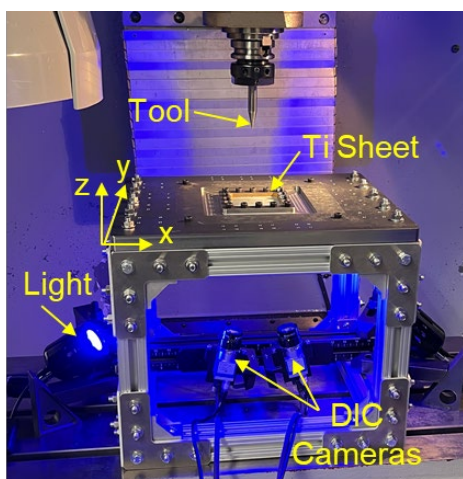


Fig. 4. SPIF experimental setup in CNC machining center.

2.3 Implant procedure

The first step in fabricating custom implants is to obtain a thin-slice (high definition) maxillofacial CT scan of the patient (an example is shown in Fig. 5). This is routinely used by the medical team for diagnosis and treatment planning, so is readily available for implant design.

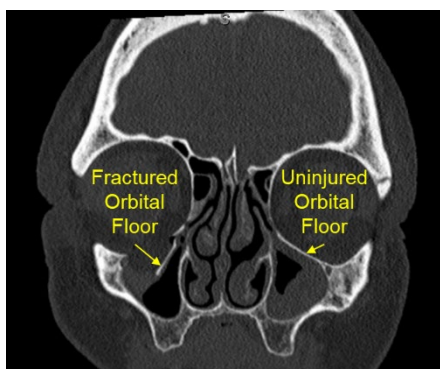


Fig. 5. Maxillofacial CT scan of the patient showing fractured and uninjured orbital floors.

The following process is optimized for patients with isolated, unilateral orbital floor fractures. CT data is used by a specially trained medical 3D lab technologist to create a 3D model in the virtual space. The intact, uninjured side is mirrored across the sagittal midline, approximately recreating the premorbid geometry of the fractured side. This mirrored geometry is then used as a template for the technologist to design a patient-specific implant. Fixation holes are added to the anterior aspect of the implant, allowing surgeons to anchor the implant to solid bone at the orbital rim. At this point, the requesting surgeon would be consulted to approve and modify the design as needed. The implant geometry is then lofted in computer-aided design (CAD) software to connect the complex implant geometry to a flat sheet to prepare it for incremental forming. A toolpath is then created, based on the lofted geometry, using computer-aided manufacturing (CAM) software to generate the machine code. The CNC machining center is prepared, as shown in Fig. 4, and then SPIF is executed to fabricate the lofted implant geometry. After forming, the implant can be extracted using a laser cutter, deburred, and then sanitized in preparation for surgery. Perforations can be added, also using the laser cutter, to promote osteointegration with the surrounding bone. If required, due to the thinness of the implant, surgeons can make minor adjustments through manual bending in the operating room. Ideally, the desired geometrical accuracy will be achieved during forming, and the need for any additional manipulation will be eliminated.

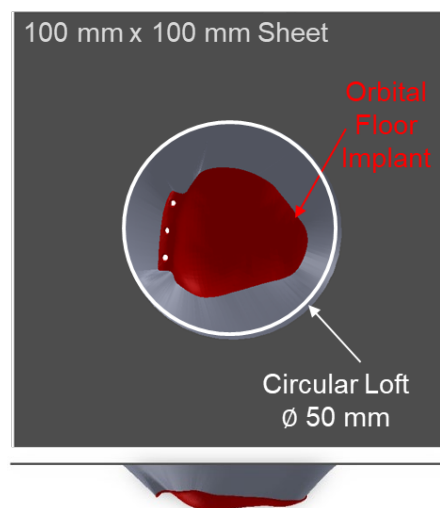


Fig. 6. CAD model of lofted patient-specific orbital floor implant geometry: (top) top view and (bottom) side view.

The geometry for this work is based on an implant designed using the above process for an adult female patient who sustained a right-sided orbital floor blowout fracture from blunt force trauma and has the geometry shown above in Fig. 6. The overall dimensions of the implant are approximately 35 mm by 28 mm with a maximum depth of approximately 11 mm prior to lofting. The three fixation holes will require an additional post-processing step after forming. A circular lofting strategy with a 50 mm diameter was used to connect the perimeter of the implant to a flat sheet in the CAD software as shown. An outside in strategy was

used for the toolpath, i.e., the lofted area was formed prior to the implant geometry.

The authors would like to thank Brian Patterson (Geisinger 3D Printing Lab) for designing the patient-specific implant and Daniel Johnson (Project Development Lab, Bucknell University) for assistance with the CNC machine setup and SPIF frame fabrication. This research is supported by the Bucknell Geisinger Research Initiative.

3 Results and discussion

One representative true stress-strain curve for each specimen orientation from the uniaxial tension experiments is shown in Fig. 7. The rolling direction (0°) has the highest strength of the three orientations studied. The longest elongation was observed for the specimens oriented at 45° with respect to the rolling direction.

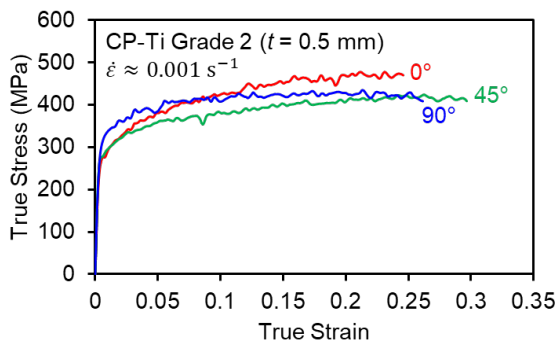


Fig. 7. True stress-strain curves for CP-Ti Grade 2 oriented at 0° , 45° , and 90° with respect to the rolling direction.

The formed orbital floor implant is shown in Fig. 8 with views from the toolside and non-toolside. The horizontal lines (shown in blue on the toolside) indicate the rolling direction of the titanium sheet. The layers of the toolpath are clearly visible on the toolpath side and create a grooved texture, particularly along the lofted geometry. Note that the lofted geometry will eventually be discarded when the implant is extracted. The implant surface on the toolside has a rough texture, which resulted in a small accumulation of chips on the part during forming. This is likely the result of the conventional milling toolpath, but further investigation and process parameter optimization are warranted. However, this rough texture may be desirable to promote osteointegration in the orbital floor region.

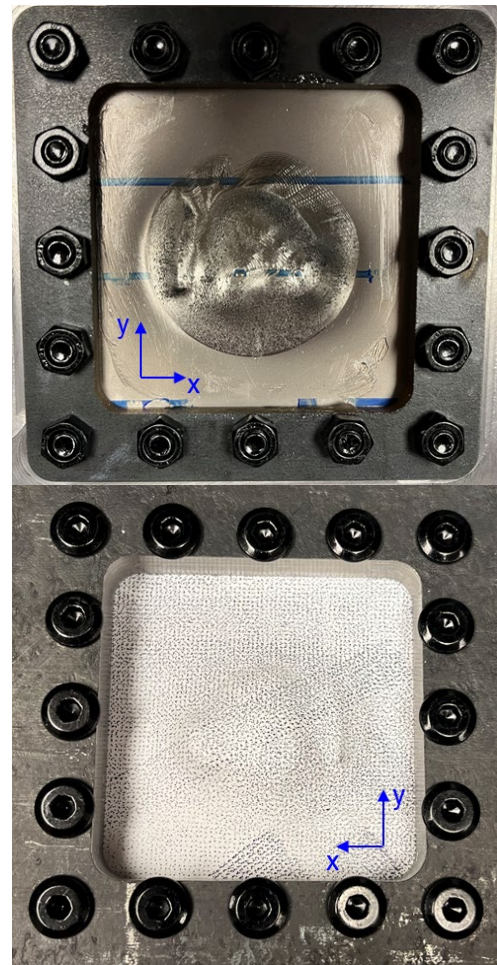


Fig. 8. Formed orbital floor implant clamped in fixture: (top) toolside and (bottom) non-toolside.

The Von Mises strain contour of the formed implant, captured on the non-toolside by the DIC system, is shown in Fig. 9. The two smaller contours that show minimal deformation near the center of the implant were the last regions to be formed as dictated by the toolpath. These regions are also visible with toolpath layer markings in Fig. 8. The correlation was lost in several locations near the fixation location at the anterior and along the posterior of the implant due to curvature of the geometry. However, the maximum recorded strain was approximately 0.265 near the posterior region.

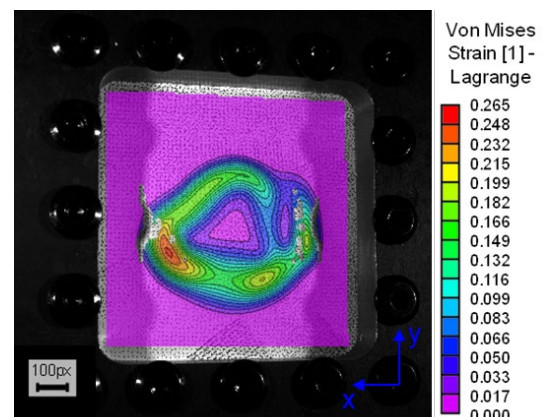


Fig. 9. Von Mises strain contour for formed component captured on non-tool side.

A 3D laser handheld scanner (Artec Space Spider) was used to create a CAD model of the formed implant while unclamped from the fixture. The target CAD implant design was imported into the postprocessing software (Artec Studio 15) and manually aligned by the user. Fig. 10 shows the resulting colormap of the geometrical deviation of the formed part from the target (CAD) geometry. The maximum deviation based on this alignment is ~ 0.78 mm near the fixation location (shown with three screw holes). This tab is typically bent by the surgeon after placement, so high precision in this location is not critical. Also, this portion of the geometry was modelled with a reverse curvature with respect to the forming direction, which is not possible with SPIF. The overall geometrical accuracy can be increased with further process parameter and toolpath optimizations that account for the springback (elastic recovery) effects after forming, unclamping, and extracting the implant.

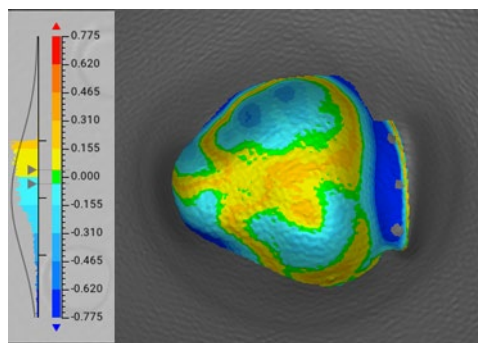


Fig. 10. Geometrical deviation of formed component from target in unclamped condition [mm].

4 Conclusions

A patient-specific orbital floor implant was designed and then fabricated using SPIF with CP-Ti grade 2 sheet specimens with an initial thickness of 0.5 mm. The CP-Ti grade 2 sheets were characterized by quasistatic uniaxial tension experiments at three different orientations. A methodology is summarized for manufacturing custom implants starting with collecting patient data and ending with implantation in the operating room. The strain was measured in-situ during SPIF using stereo-DIC on the non-tool side of the specimens. The geometrical accuracy was captured by a handheld 3D laser scanner and compared to the target CAD model.

SPIF offers an efficient, flexible manufacturing method for patient-specific implants. This work presents the first instance of an orbital floor implant manufactured using SPIF and provides evidence that SPIF can be used for much smaller implants, which require the use of thin sheets of biocompatible materials to remain lightweight while providing the required strength and geometry. Under the chosen parameters, CP-Ti grade 2 was able to be formed at room temperature, which eliminates temperature effects and a need for additional equipment. An acceptable geometrical accuracy was achieved for this first case, but further optimizations are desired. High geometric

accuracy is desired to improve symmetry in the patient's final globe position. This has both functional implications for binocular vision and aesthetic implications to restore the patient's pre-injury appearance.

Future work includes starting with perforated titanium sheets to eliminate this post processing step for the implant and optimizing the toolpath parameters to decrease the forming time and improve the surface finish of the implant. Alternative lofting strategies can also be explored to increase forming efficiency. The final thickness of the implant should be evaluated and compared to commercial implants.

References

1. M. J. Heron, K. J. Zhu, C. T. Yusuf, M. W. Njoroge, A. M. Bhagwat, A. I. Galaria, C. D. Lopez, and R. Yang, *FACE* **4**, 160 (2023)
2. M. I. Fahad and A. Z. Shammari, *Al-Khwarizmi Engineering Journal* **19**, 72 (2023)
3. G. Ambrogio, R. Conte, L. de Napoli, G. Fragomeni, and F. Gagliardi, *Key Engineering Materials* **651–653**, 925 (2015)
4. I. Bagudanch, M. L. García-Romeu, I. Ferrer, and J. Ciurana, *Rapid Prototyping Journal* **24**, 120 (2018)
5. A. Rosa-Sainz, I. Ferrer, M. L. García-Romeu, M. B. Silva, and G. C. Báez, *Key Engineering Materials* **957**, 61 (2023)
6. J. Duflou, A. Behera, H. Vanhove, and L. Bertol, *Key Engineering Materials* **549**, 223 (2013)
7. M. Sbayti, R. Bahloul, H. BelHadjsalah, and F. Zemzemi, *Int J Adv Manuf Technol* **95**, 1789 (2018)
8. H. Vanhove, Y. Carette, S. Vancleef, and J. R. Duflou, *Procedia Engineering* **183**, 174 (2017)
9. G. Ambrogio, L. De Napoli, L. Filice, F. Gagliardi, and M. Muzzupappa, *Journal of Materials Processing Technology* **162–163**, 156 (2005)
10. P. K. Bhojar and A. B. Borade, *Res. Biomed. Eng.* **31**, 352 (2015)
11. M. Sbayti, A. Ghiotti, R. Bahloul, H. Belhadjsalah, and S. Bruschi, *MATEC Web Conf.* **80**, 14006 (2016)
12. A. Rosa-Sainz, M. L. García-Romeu, I. Ferrer, M. B. Silva, and G. Centeno, *Journal of Manufacturing Processes* **86**, 66 (2023)
13. A. Piccininni, F. Gagliardi, P. Guglielmi, L. D. Napoli, G. Ambrogio, D. Sorgente, and G. Palumbo, *MATEC Web Conf.* **80**, 15007 (2016)
14. S. Thakur and S. R. Chauhan, *J. of Materi Eng and Perform* (2024)
15. KLS Martin Group, (2023)
16. ASTM International, (2024)